Computational assessment on the impact of collagen fiber orientation in cartilages on healthy and arthritic knee kinetics/kinematics

Vaishakh Raju[a] and Poornesh Kumar Koorata[a,*]

[a]Applied Solid Mechanics Laboratory, Department of Mechanical Engineering, National Institute of Technology Karnataka, Surathkal 575025, India;

*Corresponding Author

Poornesh Kumar Koorata

Applied Solid Mechanics Laboratory, Mechanical Engineering Department,

National Institute of Technology Karnataka, Surathkal 575025, India.

Email: kpkoorata@nitk.edu.in

Tel.: +91-824-247-3650

Fax: +91-824-247-4003

Abstract: 339 words

Main Text: 5732 words

Abstract

Background:

The inhomogeneous distribution of collagen fiber in cartilage can substantially influence the knee kinematics. This becomes vital for understanding the mechanical response of soft tissues, and cartilage deterioration including osteoarthritis (OA). Though the conventional computational models consider geometrical heterogeneity along with fiber reinforcements in the cartilage model as material heterogeneity, the influence of fiber orientation on knee kinetics and kinematics is not fully explored. This work examines how the collagen fiber orientation in the cartilage affects the healthy (intact knee) and arthritic knee response over multiple gait activities like running and walking.

Methods:

A 3D finite element knee joint model is used to compute the articular cartilage response during the gait cycle. A fiber-reinforced porous hyper elastic (FRPHE) material is used to model the soft tissue. A split-line pattern is used to implement the fiber orientation in femoral and tibial cartilage. Four distinct intact cartilage models and three OA models are simulated to assess the impact of the orientation of collagen fibers in a depth wise direction. The cartilage models with fibers oriented in parallel, perpendicular, and inclined to the articular surface are investigated for multiple knee kinematics and kinetics.

Findings:

The comparison of models with fiber orientation parallel to articulating surface for walking and running gait has the highest elastic stress and fluid pressure compared with inclined and perpendicular fiber-oriented models. Also, the maximum contact pressure is observed to be higher in the case of intact models during the walking cycle than for OA models. In contrast, the maximum contact pressure is higher during running in OA models than in intact models. Additionally, parallel-oriented models produce higher maximum stresses and fluid pressure for walking and running gait than proximal-distal-oriented models. Interestingly, during the walking cycle, the maximum contact pressure with intact models is approximately three times higher than on OA models. In contrast, the OA models exhibit higher contact pressure during the running cycle.

Interpretation:

Overall, the study indicates that collagen orientation is crucial for tissue responsiveness. This investigation provides insights into the development of tailored implants.

Keywords: Collagen fiber orientation; Fiber reinforced biphasic model; Gait cycle; Knee articular cartilage; Osteoarthritis;

1. Introduction

Daily physical activities like walking, jogging, and running lead to significant compressive loads on the knee cartilage, causing knee osteoarthritis (OA), especially in older people [1–4]. The articular cartilage constituents such as collagen fibers, proteoglycan matrix, and interstitial fluid collectively withstand body weight (BW) during activities like walking, running, stair climbing, and kneeling. The load on the knee joint is different for each of these activities 1BW, 1.5BW, 2BW, and 4BW, respectively [5–7]. The collagen network of articular cartilage protects chondrocytes, withstands high tensile force, and protects cartilage from rupture. This network attaches the cartilage to the subchondral bone and provides attachment for proteoglycans [8]. In the loading and unloading stages, the osmotic pressure increases in the articular cartilage, significantly increasing the interstitial fluid pressure. The body force is distributed throughout the cartilage during the loading stage and increases the shearing force on the articulating surface. Hence collagen fibers are subjected to complex loading conditions due to the interstitial fluid pressure and shearing force [9–11]. OA leads to degradation in cartilage structure in terms of fibrillation and proteoglycan depletion, hindering the mechanical characteristics of the cartilage [12–15]. To better understand cartilage degradation associated with OA, it would be convenient to characterize the collagen fiber orientations and their responses in a complex loading environment under different gait activities.

The collagen fibers in cartilage provide mechanical rigidity, which helps to maintain the solid matrix's structure. Also, the fibers are distributed heterogeneously throughout the cartilage, with their structure similar to an arcade-like design from the articulating surface to the subchondral bone [16,17]. The fibrils are oriented parallel to the articular surface in the superficial zone. However, they become more randomly oriented in the transitional zone and turn perpendicular to the bone-cartilage interface in the deep zone to firmly anchor the tissue to the subchondral bone [18–20]. The fiber orientation in the respective zones is represented with split-line patterns is the most widespread technique used in the literature [21–23].

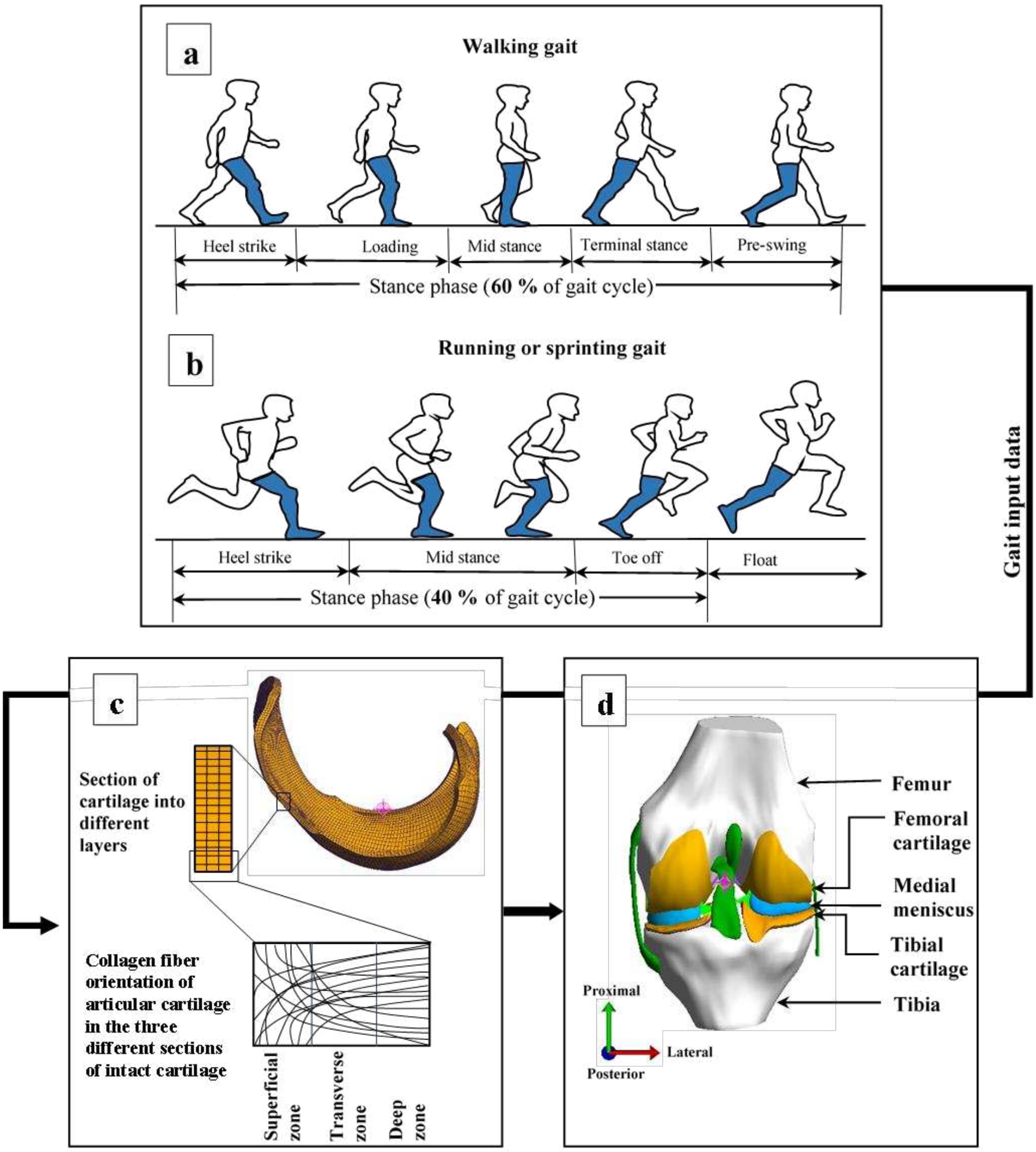

Fig. 1. Schematic of workflow: (a) the stance phase of the walking gait cycle; (b) the stance phase of the running gait cycle; (c) sagittal view of femoral cartilage with the orientation of collagen fibers in a depth-wise direction; (d) finite element model of the knee joint where the gait input data and various collagen fiber orientation models are applied.

The fiber network is known to be organized differently in healthy and arthritic cartilage. The collagen fiber orientation significantly influences the tissue response and the contact mechanism for OA cartilage [7,24]. In addition, it is reported that the tissue response is highly sensitive to fiber reorientation and loading direction [25]. Fiber reorientation is the major mechanism when loading perpendicular to collagen fiber orientation; however, when loading parallel to the fiber direction, a reduction in collagen fibers crimp and fiber reorientation occurs [26]. Hence it is necessary to understand the behavior of cartilage response with respect to the collagen fiber orientation. Even though literature is available on the tissue responses for arthritic cartilage cases, the relation between collagen fiber orientation/loading direction and tissue response is not adequately studied [3,27–29].

It is reported that depth-dependent fiber-oriented cartilage models can accurately estimate the realistic contact stress and fluid pressure in the knee joint [30]. However, the knee responses from daily activities such as walking and running by considering the depth-dependent cartilage characteristics are missing in the literature. In addition, the biphasic hyperelastic material models (neo-Hookean) available in commercial software do not capture the critical tissue response, such as the distribution of interstitial fluid pressure and shear stress [31]. However, results from the current fiber network model show an increase in the interstitial fluid pressure on the contact surface and could capture it during knee loading.

Also, the orientation of collagen fibers is crucial to the mechanical responses of connective tissue and load-bearing tissue because it serves as the tissue's structural foundation [32]. The study of the mechanics of collagen fiber orientation advances the understanding of the mechanism of tissue formation from scratch. However, there is currently a lack of knowledge regarding the mechanism behind fiber orientation. Also, the literature results suggest that collagen orientation plays a critical role in soft tissue response during load transmission of the knee joint [26]. Hence, the present study's objective is to investigate how collagen fiber orientation affects the mechanical response of the cartilage during the gait cycle. Moreover, the walking and running knee responses are calculated for the parallel and perpendicular loading conditions with respect to the collagen fiber alignment. We hypothesise that the vertical collagen fiber-oriented network plays a significant role in supporting and protecting articular cartilage. Damage to this network would affect the mechanics of the joint and increase the tissue's susceptibility to OA. Multiple oriented cartilage models are created and analysed for various gait cycles. The results help researchers to develop better assistance devices for arthritis patients for subject-specific activities like walking and running. Additionally, this research contributes to developing subject-specific composite knee implant material with depth-dependent features by implanting fibers in particular orientations following the activity requirements.

2. Methods

2.1 Finite Element Model

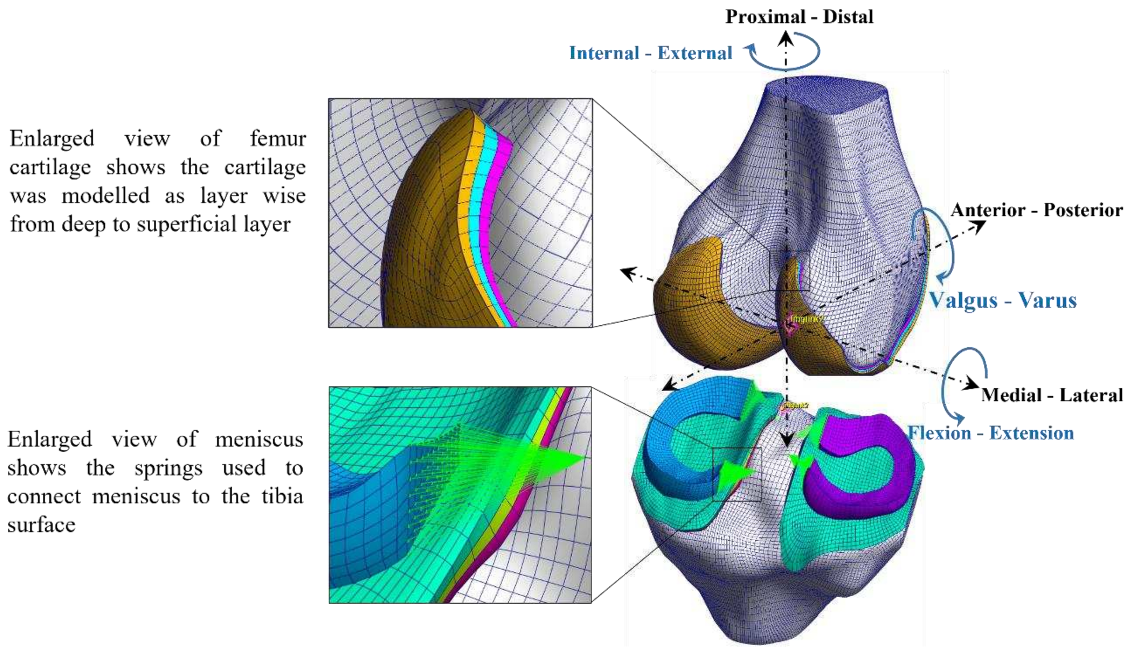

Fig. 2. The schematic diagram of the finite element model shows that the gait input data (forces and rotations) are applied on all 6 degrees of freedom of the knee joint through the three mutually perpendicular axes.

A case study is performed based on open-knee geometry [33], simulating the walking and running cycle to study the influence of collagen fiber orientation in multiple gait activities. The tibiofemoral joint is segmented from a female subject (70 years, 77 kg) into femur, tibia, collateral ligaments (MCL and LCL), cruciate ligaments (ACL and PCL), menisci (lateral and medial), and cartilage (femoral and tibial) as given in Figure 1. The finite element model of the knee joint is imported in FEBio Studio 1.2.0 (University of Utah and Columbia University) an open-source finite element analysis software and static analysis is performed [34].

The soft tissues and bone are discretized into 56,433 hexahedral elements and 25,220 shell elements. The soft tissues such as cartilage, ligaments and meniscus are meshed with hexahedral brick elements (HEX8), and the bones such as tibia and femur are meshed with shell elements (QUAD4). A mesh convergence test is carried out to ensure that the solution shouldn't change when the mesh is refined. Multiple iterations are performed on the model from element length 0.5 to 2 mm in 0.5 mm increments. The optimum element length calculated for generating the same contact pressure on the surface is approximately 1 mm. Also, the software's mesh inspector is used to refine the model and ensure no stress or strain singularities. The current study, however, assumes each layer's mesh size is the same for numerical convergence purposes. The cartilage is divided into three layers in the direction of cartilage thickness, from the superficial layer to the deep layer shown in Figure 2. The Meniscal attachment to the tibia is modelled using a set of linear springs with a total spring constant of 350 N/mm at each meniscal horn. Eighty-eight linear springs are attached to the tibial plateau at each horn attachment. The spring constants of each spring are calculated using Eq. (1), where k is the stiffness of each spring, E is the elastic modulus of the meniscal horn, A is the total horn face area, and N is the number of nodes on that face [35–38].

$$k = \frac{EA}{NL} \tag{1}$$

The 3D geometry used for the present investigation is segmented from a 70-year-old subject, the cartilage and other soft tissues are intact, and no evidence of arthritis is reported in the source [33]. Also, there might be a difference in the thickness of cartilage and ligaments of the current geometry due to pathological conditions compared with younger subjects. This may cause a slight variation in mechanical response compared to the actual response. This is a significant limitation of subject-specific finite element model studies like this. Researchers also developed an instrument to evaluate the methodological quality for subject-specific finite element studies dedicated to orthopaedics. This can make it easier to assess the quality in the systematic reviews of finite element models [39].

2.2 Gait input data

The gait input data (forces and rotation) are applied to the knee joint through the three mutually perpendicular axes shown in Figure 2. In this work, the gait data are taken from the literature and imported into the model for simulation [40–44]. Six different but simultaneous movements occur between the femur and tibia during the walking and running gait cycle. It is divided into three rotations (extension–flexion, internal-external, and varus-valgus) and three force components (anterior-posterior, medial-lateral, and proximal-distal) [45].

The walking kinetic and kinematic data are obtained from a subject (28 years old male, 82 kg) who walked on a 10 m track at an average speed (of 1.7 m/s) [28]. The typical human walking speed is between 1.2 m/s and 1.4 m/s, but the present study uses data from the literature that the subject's average walking speed is 1.7 m/s. The running data were obtained from a subject (22 years old male, 76 kg average) running at 4.07 m/s in a 30 m walkway [46]. The authors of both studies used 3D motion capture and anatomical marker systems to track walking and running data and converted them into knee kinetics and kinematics data with commercial software.

The walking gait data are adapted from a young, healthy subject, whereas the structure of the knee tissues developed from a pathological, aged subject. Also, the gait pattern of younger adults varies from that of older subjects, even with good health conditions, due to differences in knee extension and shorter stride length [47,48]. In the present work, the gait data are taken from young individuals with longer stride lengths (1.7 m/s), even though the height of an individual also changes the gait pattern [49]. Hence such pre-clinical work without the study of in vivo models is another limitation of the work. In addition, the weight of the knee model and the applied load measured from the human subject are different. Nevertheless, this weight mismatch will not affect the results significantly since the tissue response mainly depends on the gait input data and the cartilage material model. Since the same geometry is used in all subject cases, the study focuses primarily on the tissue response to various activities. Parametric modelling technology can be used to overcome the mismatching between applied load and knee joint weight. This technique can quickly build models to overcome weight mismatching limitations [50]. This can be considered in future research with orthopaedic modelling limitations.

2.3 Contact and boundary conditions

In the model, the tibia is constrained in all degrees of freedom, whereas the femur is subjected to rotation for the gait input data. Also, translational forces are applied to the femur. The interaction between cartilage-cartilage and cartilage-meniscus is set to be frictionless. The meniscus is connected to the tibial surface with elastic springs to mimic the anterior and posterior horn attachment.

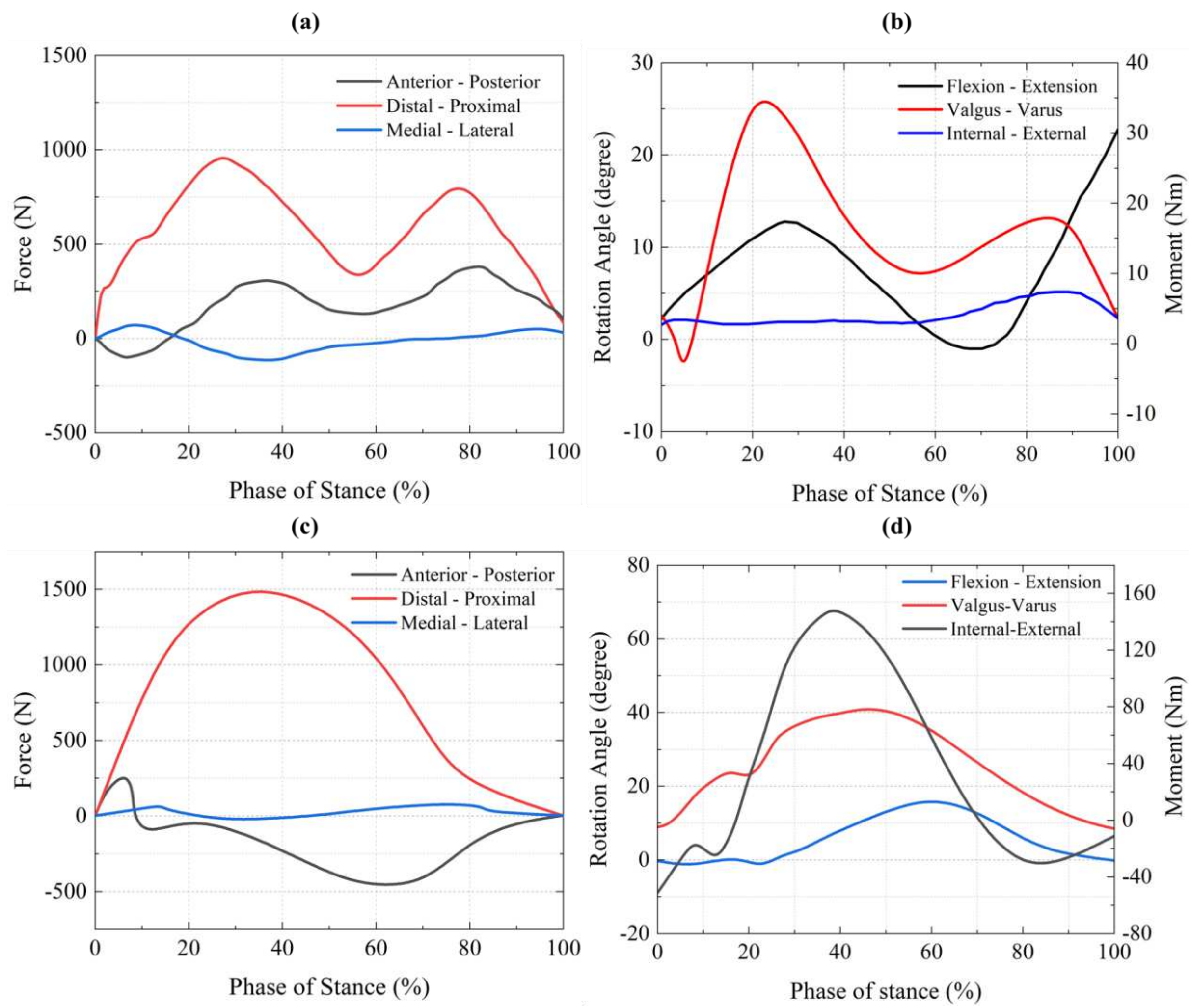

Fig. 3. Input gait data for the analysis: (a) the components of forces (N) act on the knee joint in all three degrees of freedom during the stance phase of the walking gait cycle; (b) the rotation angle (degrees) in the sagittal plane (flexion-extension), frontal plane (valgus-varus or abduction-adduction) and transverse plane (internal-external) respectively during the stance phase of walking cycle [28]; (c) the forces as acting on the knee joint during the running gait (d) the rotation in all three plains of the joint during running gait [46].

At the initial simulation stage, the cartilage and meniscus are made to make light contact to achieve the initial convergence. A displacement-controlled input is applied to the femur to achieve convergence for attaining the initial contact. Also, the contact between ligament-ligament and ligament-cartilage is chosen as frictionless. Following the initial conditions, forces and rotations applied during the stance phase of the gait cycle through a cylindrical joint in the analysis. The tibia is fixed in space for the entire analysis time. The femur is prescribed the corresponding gait input data in all three linear and rotational directions for a time frame of 0–1.5s for the walking cycle. Similarly, the corresponding force and rotation data are applied to the femur for a time frame of 0–1s for the running cycle. The forces (proximal-distal, anterior-posterior, and medial-lateral) and rotations (flexion-extension, valgus-varus and internal-external) during the stance phase of the gait cycle for walking and running applied to the model are given in Figure 3.

2.4 Material models

The soft tissue is divided into fibrillar (collagen fibers) and non-fibrillar (proteoglycan matrix and interstitial fluid) components [17]. To simplify the model, the inhomogeneous compressive modulus of the matrix is neglected [51,52]. A fiber-reinforced porous hyperelastic (FRPHE) model is used for implementing the biphasic articular cartilage tissue (femoral and tibial cartilage). The collagen fibers are embedded in the ground matrix since fibers can only withstand tension and cannot sustain on their own. A fiber with exponential power-law provided by Eq. (2) is utilised to model the collagen fibers. A neo-Hookean compressible hyperelastic material model given by Eq. (4) is employed to model the proteoglycan ground matrix. The strain-dependent permeability nature of tissue is implemented based on the Holmes-Mow model given by Eq. (5) [53–62].

The fiber strain energy density function is given by,

$$\psi = \frac{\xi}{\alpha\beta}\left(\exp\left[\alpha\left(I_n - 1\right)^{\beta}\right] - 1\right) \tag{2}$$

$$N = \sin\varphi\cos\theta e_1 + \sin\varphi\sin\theta e_2 + \cos\varphi e_3 \tag{3}$$

Where $I_n = \lambda_n^{\,2} = N.C.N$, λ_n = the fiber stretch, N = the fiber orientation represented by θ and φ [deg] given by Eq. (3), ξ = representing a measure of the fiber modulus [MPa], α = coefficient of exponential argument, β = power of exponential argument (fiber nonlinearity), θ, φ = spherical angle for fiber orientation [deg].

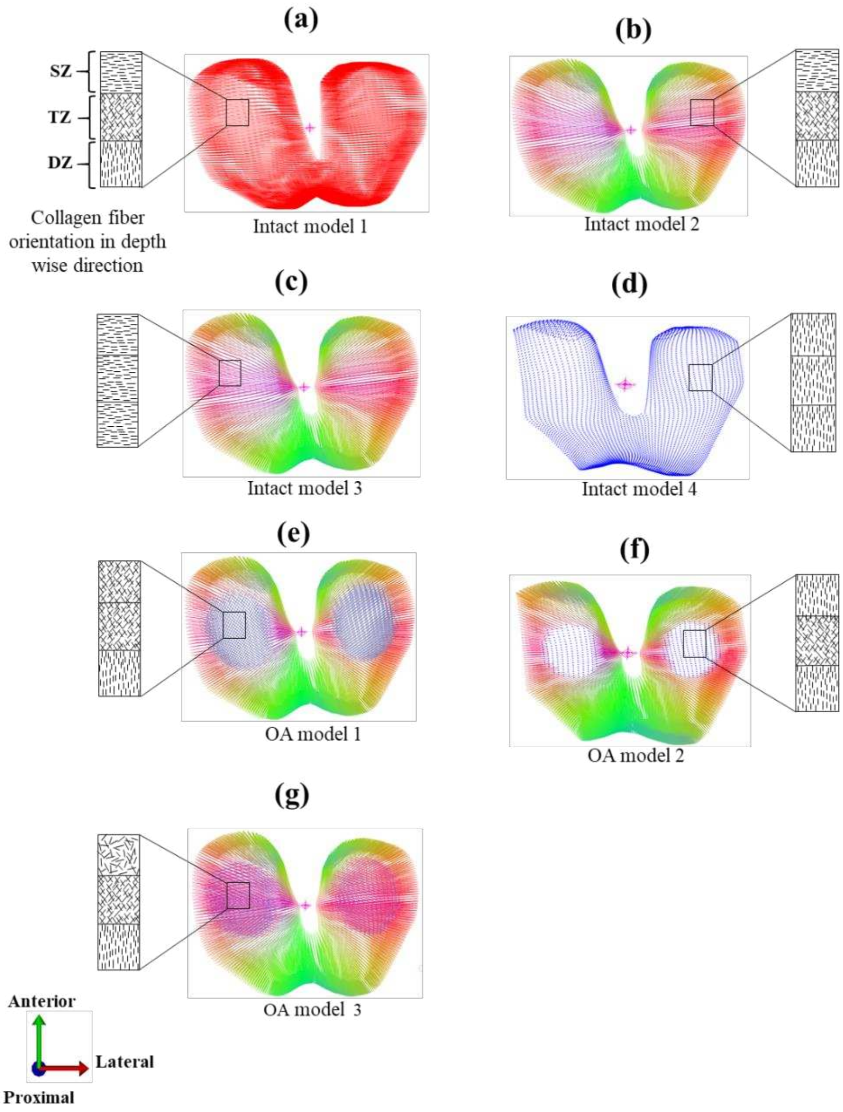

Fig. 4. Different femoral cartilage models based on distinct collagen fiber orientation are represented using the split-line pattern. (a-d) shows the intact cartilage model, and (e-g) represents osteoarthritic models. The fiber orientation in the depth-wise direction is shown in the boxes.

The proteoglycan matrix strain energy density function (Mooney-Rivlin) is given by:

$$\psi = C_1(I_1 - 3) + C_2(I_2 - 3) + \frac{1}{D}(\ln J)^2 \tag{4}$$

where C_1, C_2, D are hyperelastic material constants, when $C_2 = 0$ the model reduces to neo-Hookean constitutive model, I_1, I_2 are the first and second invariants corresponding to the left Cauchy-Green deformation tensor, J is Jacobian of the deformation given by $\det(F)$, and F is the deformation gradient. $D = 2/K$ and $C_1 = \mu/2$ where K is the bulk modulus and μ is the shear modulus. The strain-dependent permeability of soft tissue is described using the Holmes-Mow constitutive equation given in Eq. (5) and Eq. (6) [59,62,63].

$$K_s = k(J)I \tag{5}$$

$$k(J) = k_0 \left(\frac{J - \varphi_0}{1 - \varphi_0} \right)^{\alpha_1} e^{\frac{1}{2}M\left(J^2 - 1\right)} \tag{6}$$

Where $k(J)$ is a strain-dependent component, k_0 is isotropic hydraulic permeability, M is an exponential strain-dependent co-efficient and α_1 is a power-law exponent. The inhomogeneity in the solid phase of the tissue is modelled by varying the volume fraction along the thickness direction. The solid volume fraction φ_0 is given in Eq. (7), where z varies from 0 to 1 from cartilage surface to subchondral bone [64].

$$\varphi_0 = 1 - (.8 - .15z) \tag{7}$$

Seven different femoral and tibial cartilage models are created to investigate the influence of collagen fiber orientation in the superficial zone and depth direction for an intact and arthritic knee. The femoral cartilage models created are shown in Figure 4. The first four models represent the intact knee, and the rest three the arthritic knee cases. The collagen fiber orientation is defined using split-line patterns, and the direction of the fibers is controlled using the model. The split-line patterns are obtained from the literature [21,23,30,65–67].

Table 1. Material constants for FRPHE intact and arthritic cartilage models (intact model-1 and OA model-1).

Material Constants		**Intact knee**			**Arthritic knee**			**Source**
		Deep zone	**Middle zone**	**Superficial zone**	**Deep zone**	**Middle zone**	**Superficial zone**	
Collagen fiber: (Fiber exponential power uncoupled)	**ξ** (MPa)	9.19	4.595 4.595	9.19	4.595	2.297 2.297	4.595	[30,56]
	α	0	0	0	0	0	0	
	β	2	2	2	2	2	2	
	Θ (deg)	0	0 0	0	0	0 0	0	
	φ (deg)	0	45 -45	90	0	45 -45	90	
Proteoglycan matrix: (compressible hyperplastic neo-Hookean)	**μ** (MPa)	1.82	1.82	1.82	0.91	0.91	0.91	[55]
	K (MPa)	1860	1860	1860	930	930	930	
Interstitial fluid: Permeability (Perm-Holmes-Mow)	K_o (mm^4/Ns)	.00174	.00174	.00174	.00174	.00174	.00174	[59,63]
	M	7.1	7.1	7.1	7.1	7.1	7.1	
	α	2	2	2	2	2	2	
Density	ρ_s ($tonnes/mm^3$)	1×10^{-9}	1×10^{-9}	1×10^{-9}	1×10^{-9}	1×10^{-9}	1×10^{-9}	
	ρ_f ($tonnes/mm^3$)	1.5×10^{-9}	1.5×10^{-9}	1.5×10^{-9}	1.5×10^{-9}	1.5×10^{-9}	1.5×10^{-9}	[52]
Volume fraction	φ_0	0.2	0.275	0.35	0.2	0.275	0.35	

i) In intact model-1, the split lines are aligned in the medial-lateral direction in the femur and tibial cartilage. The split-line representation is shown in Figure 4(a). The model-1 mimics the arcade-like collagen structure.

ii) In intact model-2, the split lines are aligned in the plane of the articulating surface, and the direction is pointed outward from the centre according to the geometry illustrated in Figure 4(b). Also, the orientation along the depth-wise path mimics an arcade-like structure.

iii) In intact model-3, the split line pattern is aligned similar to model-2; It is the same for all three zones, as shown in Figure 4(c).

iv) In the intact model-4, the split-line pattern is aligned along the proximal-distal direction, as shown in Figure 4(d), and it is the same for all zones.

The arthritic zone where fibrillation occurs for the osteoarthritic cartilage model is selected. The split-line pattern orientation is assigned to obtain the influence of collagen orientation in the OA knee. Three different OA models are used to investigate the impact of collagen fiber orientation.

v) The split-line pattern is aligned such that it is equally inclined to the medial-lateral and proximal-distal axis in OA model-1. Also, the alignment is restricted inside the arthritic zone, as shown in Figure 4(e).

vi) The split-line pattern is aligned in the proximal-distal direction, as shown in Figure 4(f) in OA model-2.

vii) The OA model-3 represents the random split-line orientation of collagen fibers, as shown in Figure 4(g).

The properties of the FRPHE cartilage material are implemented into the model according to Table1. Even though some of the proteoglycan matrix parameters are chosen as constant throughout the depth of the tissue, the depth-dependent heterogeneity is applied based on the matrix's strain-dependent permeability characteristics, which are represented using Equations 4-6. Also, the depth-dependent attributes of the solid material (proteoglycan matrix) and fluid (interstitial fluid), such as density, are chosen as the same throughout the depth to simplify the model. The collagen fibers are assumed to be oriented perpendicular or inclined to the articular surface of the cartilage for severe OA conditions compared with the intact case. This orientation affects the tissue response, and it is believed that these multiple-oriented collagen models may predict the actual tissue response due to the change in direction. These fiber orientation changes are named fibrillation, reported in the literature [23,68].

The menisci, collateral, and cruciate ligaments are modelled as transversely isotropic poroelastic, and the constants are chosen from the literature [69–72]. Another limitation of this study is that even though the meniscus and ligaments are made of fiber-reinforced poroviscoelastic material, they were represented using transversely isotropic poroelastic material. However, this simplification of the model aids in resolving the analysis's convergence problem when impact-loading scenarios like running and walking are present. In the current investigation, the transversely isotropic viscous menisci tissue and fiber-reinforced viscous cartilage interchange fluid may impact the cartilage's interstitial fluid pressure. This change in interstitial fluid pressure can affect the cartilage's stress, strain, and contact pressure distribution due to the dissipated mechanical energy during the cyclic compression on the meniscus. Meanwhile, the alteration brought on by the results from other tissue types is disregarded, which is another limitation of the work. The present study focuses on the mechanical response of fiber-reinforced cartilage tissue rather than other tissues. Additionally, the literature implies that transversely isotropic material can be an alternative to fiber-reinforced material in predicting tissue responses [72–74].

3. Results

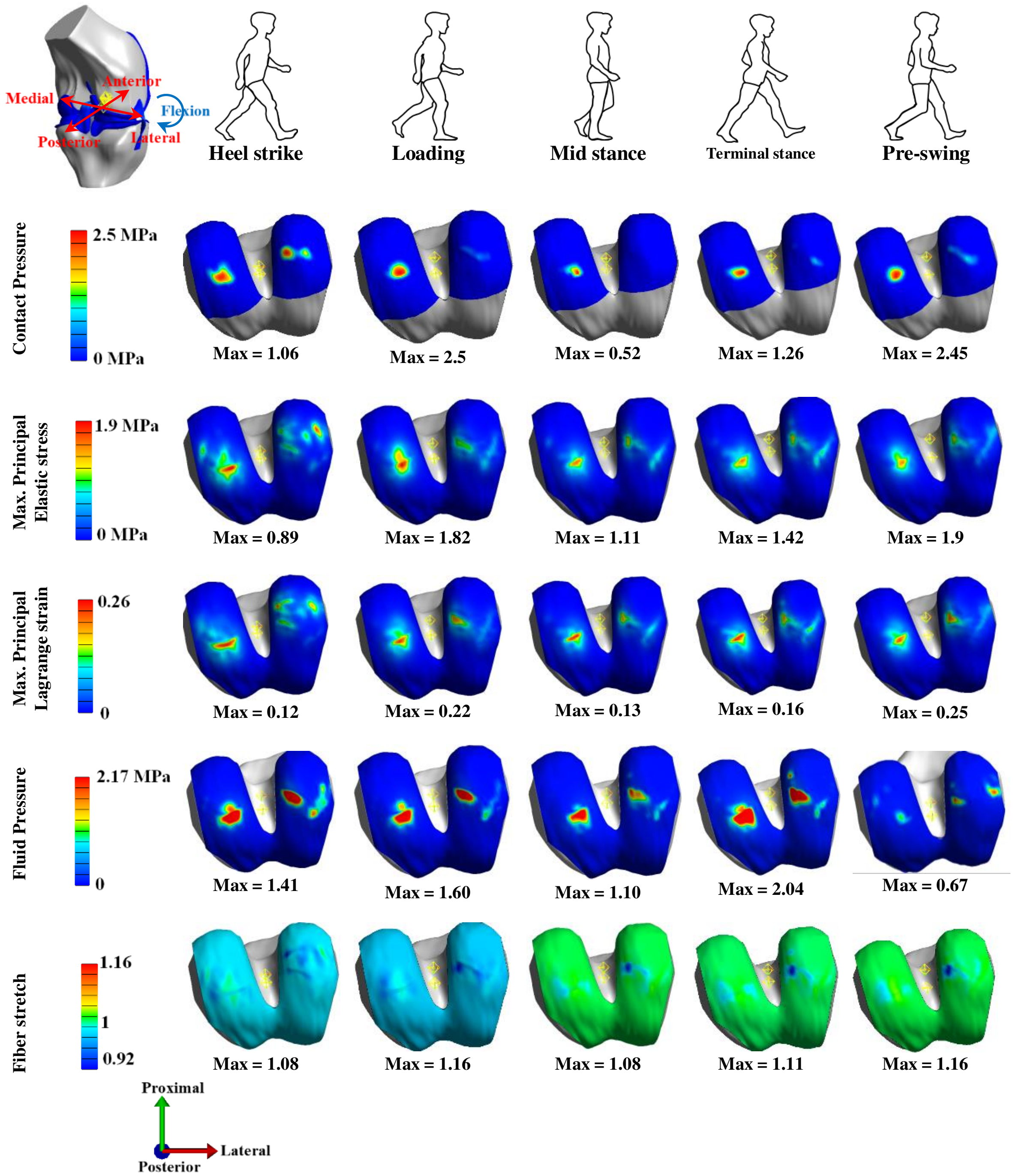

Fig. 5. Contours of mechanical responses of femoral cartilage on the surface of intact model-1 during the stance phase of walking (60% gait cycle).

Figure 5 shows the contours of different mechanical responses of the femoral articular cartilage during the stance phase of the walking gait cycle. It displays the variation in various mechanical responses, such as contact pressure, principal elastic stress, Lagrange strain, fluid pressure, and fiber stretch of the biphasic cartilage. Throughout the cycle, it is seen that the contact pressure generated on the articulating surface varies, and maximum contact pressure of 2.5 MPa is observed at the end of the heel strike on the lateral side. According to published research, osteoarthritis is most prone to develop on the articulating surface where the maximum contact pressure is generated [75].

Figure 6 depicts the contours of various mechanical responses throughout the running gait cycle. However, this also shows a similar trend in the contact pressure, as the maximum value of 2.9 MPa is observed at the end of the heel strike. The maximum contact pressure on the articulating surface of the cartilage during walking and running cases is 2.5 MPa and 2.9 MPa. On the waking cycle, the maximum values are at 30% and 90% of the stance phase, whereas on the running cycle, the maximum value is obtained at 40%. Figures 1(a) and 1(b) shows the loading and the terminal stance of the gait cycle are the stances where the highest percentage of body weight acts on the knee joint during walking. In a gait cycle, these stances are situated at roughly the 30% and 90% positions of the stance phase. Thus, there is a chance that the area will experience the maximum mechanical responses. Similarly, during a running cycle, the maximum body weight that can bear on the knee joint is at mid-stance during the stance phase. Also, the trend of tissue responses for both cases is entirely different during the gait. The mismatch in trends between mechanical responses between loading and terminal stances may be due to the percentage of body weight acting on the knee joint during the respective stances. Also, the mismatch in the mechanical responses between walking and running gait may be due to the variation in the magnitude of body weight acting on the knee joint for walking and running. The maximum elastic stress and Lagrange strains are concentrated in the lateral-medial epicondyle area of the femoral cartilage during walking gait; however, during the running gait, these maximum values are observed in the posterior side of the knee cartilage.

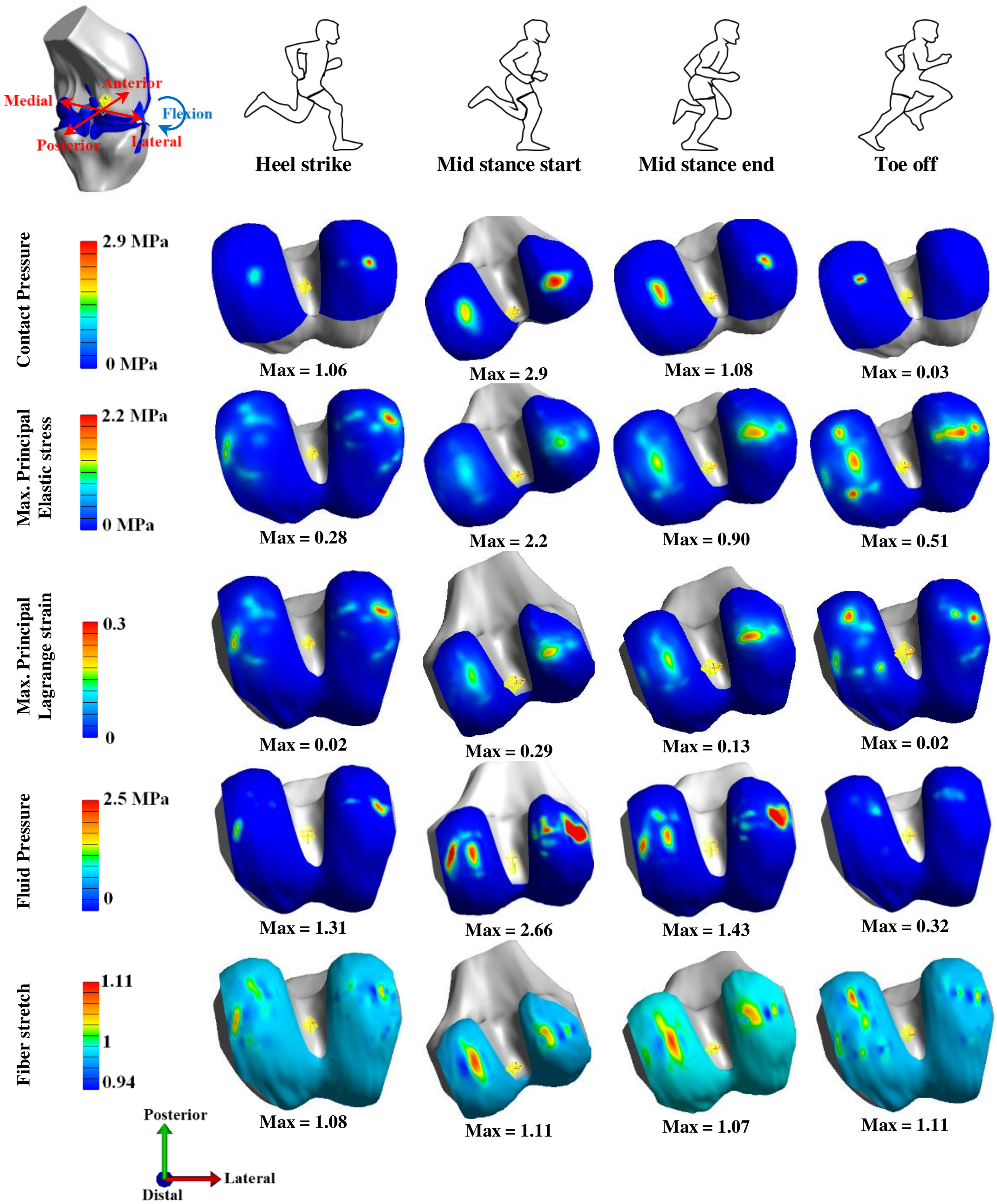

Fig. 6. Contours of mechanical responses of femoral cartilage on the surface of intact model-1 during the stance phase of running (40% gait cycle).

Further, maximum principal stress of 1.82 MPa is produced throughout the walking cycle, which is more than the fluid pressure of 1.60 MPa that is produced during the loading stance (first peak in the loading curve). However, the principal stress produced at the terminal stance, 1.42 MPa, is less than the fluid pressure, 2.04 MPa (second peak in the loading curve). A fluid pressure of 2.66 MPa is produced during the running cycle at the mid-stance start (the maximum peak in the loading curve), which is more than the maximum primary stress of 2.20 MPa produced. The medial side of the femoral cartilage experiences the maximum stresses and strains during the whole stance period of the walking gait. In contrast, the lateral compartment of the cartilage has the maximum responses during the running gait. The collagen fiber stretch also changes during the stance phase, with most variation seen in the running rather than walking cycle.

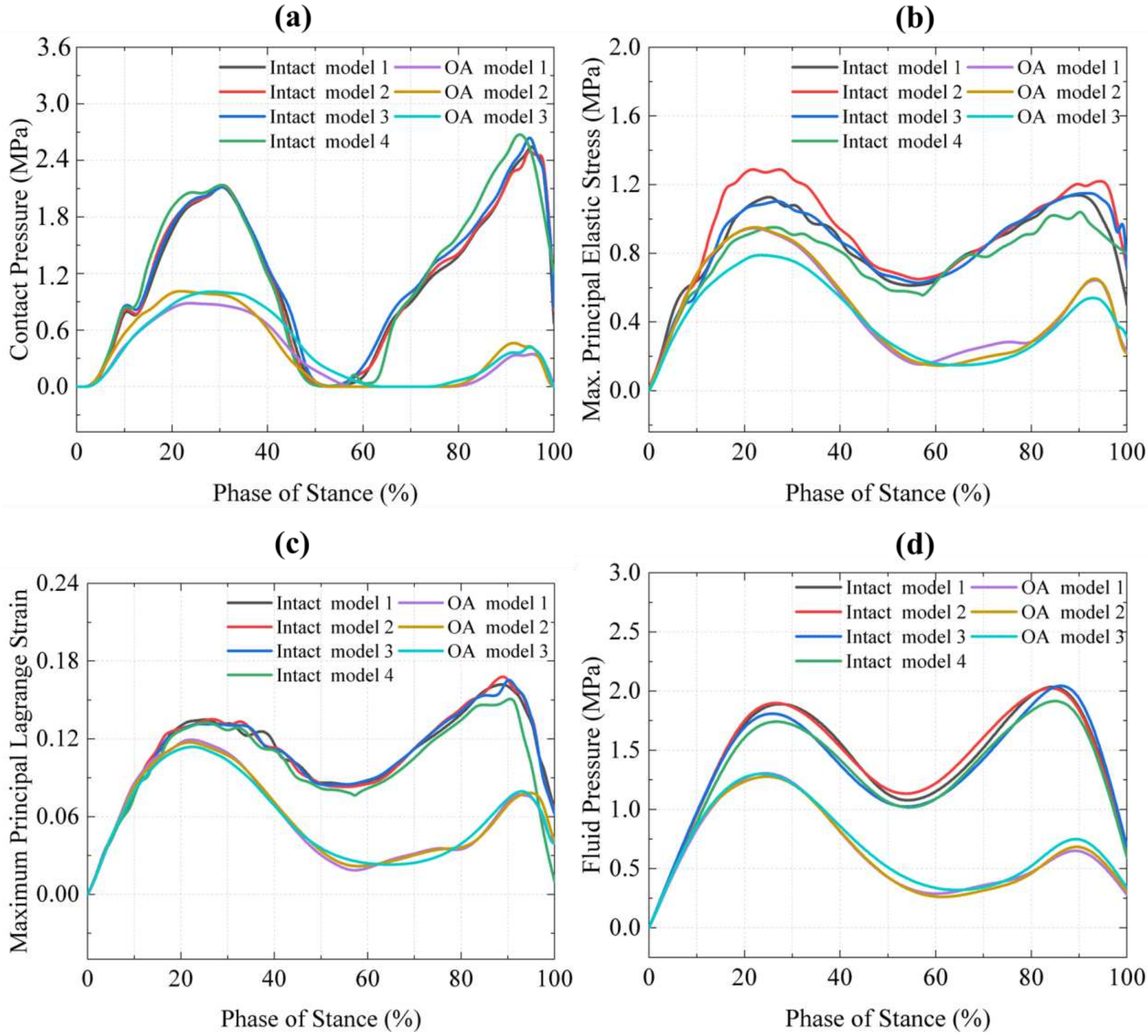

Fig. 7. The comparison of mechanical characteristics of cartilage for different models during the stance phase of walking gait: (a) the contact pressure generated on the articulating

surface; (b) maximum principal elastic stress produced on the articular zone; (c) maximum principal Lagrange strain; (d) maximum fluid pressure generated in the biphasic cartilage.

Figure 7 shows the variation in mechanical responses for different collagen fiber-oriented models during the stance phase of the gait cycle. All intact and arthritic models show similar trends in contact pressure, maximum principal elastic stress, maximum principal Lagrange strain, and fluid pressure. The maximum contact pressure generated on OA cartilage is higher than the intact cartilage model during the running cycle. However, the intact model observes elevated contact pressure during the walking cycle. The study indicates that running degrades cartilage morphology as peak contact stresses rise. Also, it is well known that OA can cause the cartilage's surface layer to deteriorate. Hence, the contact pressure produced by the OA model, where collagen fibers orientated normally to the articulating surface at the cartilage-cartilage interface, can be greater than in the intact model, where collagen fibers are parallel to the articulating surface at the cartilage-cartilage interface.

The intact model aligned with the proximal-distal direction has a higher contact pressure than the other models shown in Figure 7(a). Also, there is a 200% difference in the contact pressure for intact and OA models, and contact pressure reaches zero during the mid-stance (40-60% of the stance phase) for both models. In the walking gait, two contact pressure peaks are observed (during the 30% and 90% stance phases, respectively). During the first peak, contact pressure for intact models is two times higher than for OA models, and during the second peak, it is five times higher. Figure 7(b) shows higher principal stress for the intact parallel split-line model and lower principal stress for the random split-line oriented OA model during walking gait. According to previous experimental research, Green-Lagrange strain is a crucial indication of cell damage compared to other results such as contact pressure, principal stress, and fluid pressure [76,77]. Figure 7(c) shows that the maximum principal Lagrange strain has higher values for intact models than OA models. One can observe that the difference in strain between these two sets of models significantly increases from 20% to 90% of the phase of stance. Figure 7(d) shows maximal interstitial fluid pressure in soft tissue. As expected, intact models give rise to higher fluid pressure than OA models. Among intact models, models 1 and 2 (parallel-oriented collagen fiber models) show elevated responses.

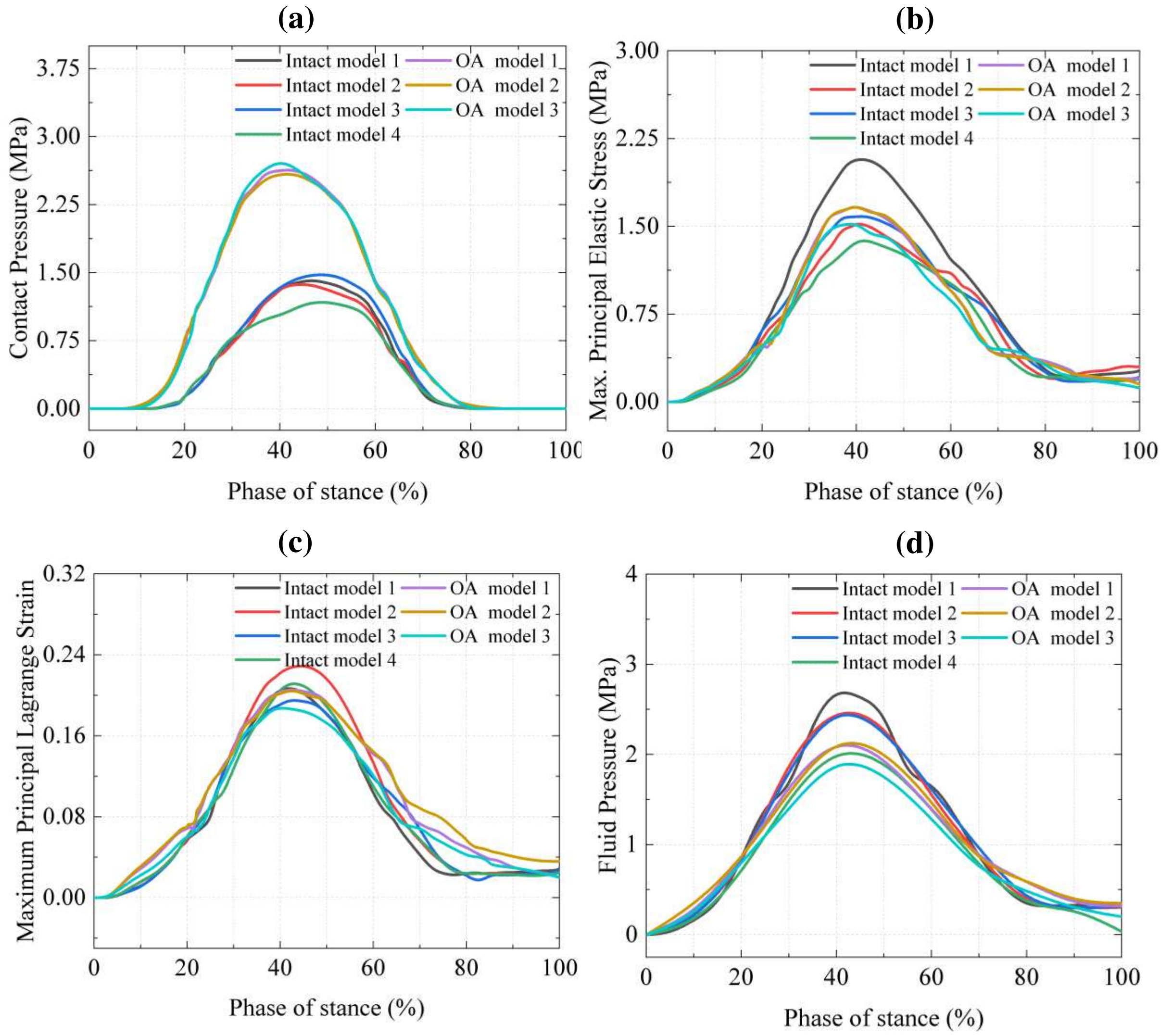

Fig. 8. The comparison of mechanical characteristics of cartilage for different models during the stance phase of running gait: (a) the contact pressure generated on the articulating surface; (b) maximum principal elastic stress produced on the articular zone; (c) maximum principal Lagrange strain; (d) maximum fluid pressure generated in the biphasic cartilage.

Figure 8 illustrates the mechanical responses of various models throughout the running gait. Even though the mechanical responses for both the walking and running cycles are comparable to the gait input data, it is interesting to note that the contact pressure created during the running cycle is more significant for the OA model than the intact model (Figure 8(a)). Also, the maximum contact pressure generated is higher for the randomly oriented OA model (OA model 3) and the minimum for the perpendicularly oriented intact model (Intact model 4). Further, it can be observed that the contact pressure for walking gait (Figure 7(a)) is strikingly high for intact models than for OA models, which is not the case for running gait.

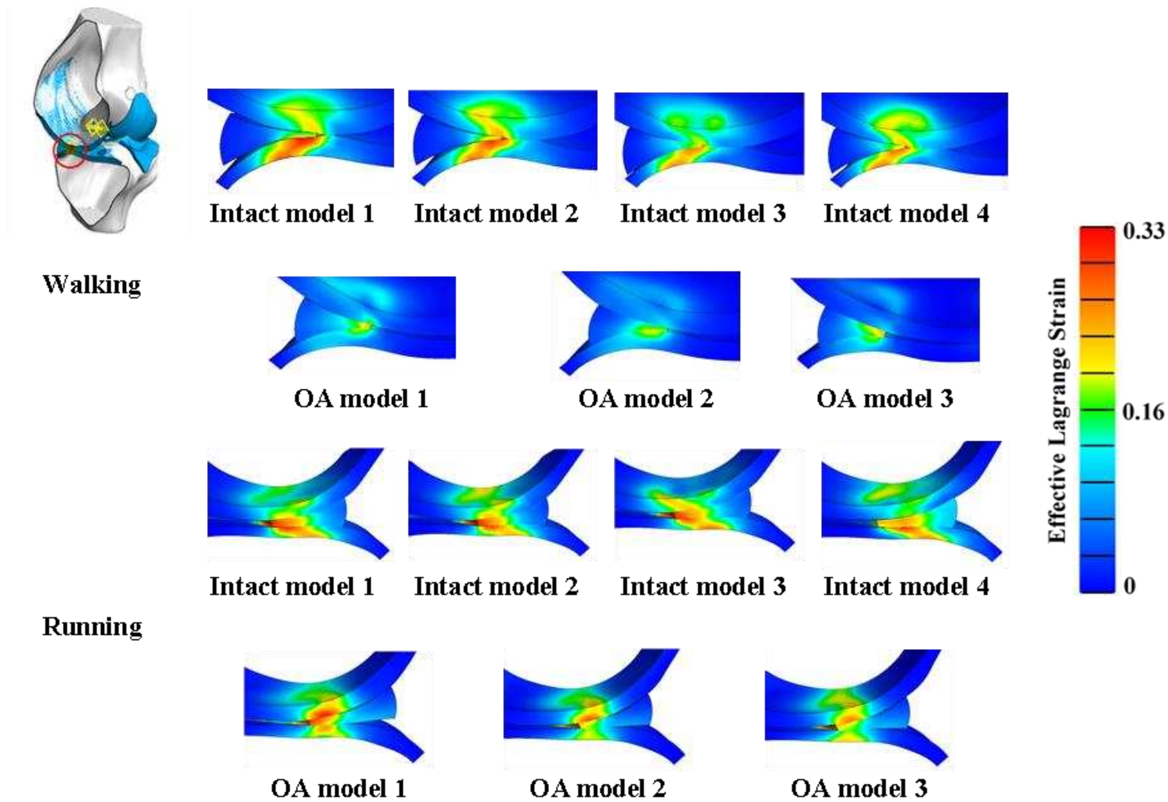

Fig. 9. The effective Lagrange strain in the sagittal plane sectional view of the articulating region (femur cartilage-meniscus-tibial cartilage interface) of the knee joint at the maximum loading position during the stance phase of walking and running gait.

Figure 8(b) shows elastic stress distribution, where the parallel split-line model (Intact model 1) exhibits the highest elastic stress, whereas the proximal-distal aligned model exhibits lower elastic stress. The Lagrange strain is plotted in Figure 8(c). One can observe that the strain distribution trend is almost similar for all the simulated cases. This response differs greatly from the walking gait scenario (Figure 7(c)). Like the Lagrange strain, interstitial fluid pressure in Figure 8(d) also shows a similar trend. However, a closer observation indicates an increase of ~ 40% in fluid pressure in the case of intact models with parallel-oriented intact models experiencing higher fluid pressure than perpendicular or inclined ones.

Figure 9 shows the effective Lagrange strain in the femoral-tibial cartilage and meniscus contact region for walking and running cases. During the walking cycle, the tibial cartilage exhibits a higher strain in the case of intact models, while only the meniscus has a higher strain in OA models. Conversely, during the running cycle, the meniscus shows a higher strain in the case of intact models, and the femoral cartilage exhibits a higher stain in the case of OA models. In addition, it can be observed that the inclined intact model-3 shows lower tibial cartilage strain than the parallel-oriented models during the walking case and during the running cycle, the perpendicularly oriented intact model-4 exhibits lower tibial cartilage strain. Further, during the running cycle, the maximum strain is detected in the tibial cartilage-meniscus interface for intact models, whereas the maximum strain is observed in the femoral cartilage-meniscus interface for OA models.

4. Discussion

A subject-specific knee geometry with six degrees of knee kinetics and kinematics data concerning walking and running gait is utilised for the present knee investigation. An FRPHE cartilage model with control on collagen fiber orientation and osteoarthritic characteristics are used for the analysis. Also, different fiber-oriented cartilage models are created for intact and osteoarthritic cases. The model determines contact pressure in the articulating area, principal stress, Lagrange strain, interstitial fluid pressure, and cartilage fiber stretch, all of which are essential factors in the evaluation of cartilage degradation [13,73,78–80]. The findings imply that the collagen fibril orientations, as revealed by split lines, play a significant role in regulating cartilage strains and stresses.

The experimental investigation by [81] predicted larger contact pressures during the heel strike on the medial compartment compared to those on the lateral compartment, which is consistent with our model. Our model yielded contact pressures of 2 and 3 MPa at the lateral and medial compartments, respectively, at 50% of the stance phase (1500 N). These values are also in the same range as those found in past computational studies (1-5 MPa with loads between 1000 and 1800 N) [75,82–87].

In the gait input data for knee kinetics and kinematics, forces and rotations corresponding to particular activities are applied to the FE knee model [88–92]. One limitation of the approach is that it uses a small displacement and rotation in the initial step to bring the model into contact with the cartilages and meniscus to achieve initial convergence. Moment-driven and rotation-driven are the two methods used to input flexion-extension, valgus-varus, and internal-external rotations to the knee model [93,94]. However, the present study uses a rotation-driven method to implement knee rotations, as shown in Figures 3(b) and 3(d). Also, it is unclear whether the FE model should be driven by a moment or a rotation because both methods predict identical measures in the literature [75].

The peak mechanical response magnitudes of the intact models are substantially more extensive than the OA model during walking gait, as shown in Figure 7; while running, peak magnitudes are observed for OA cases. Regarding the contact pressure produced, OA models have higher values than the intact model during running. The research shows that running worsens cartilage structure as the peak contact stresses increase. Additionally, it's generally understood that OA can worsen the cartilage's outer layer. As a result, the contact pressure created by the OA model, in which collagen fibers are typically oriented to the articulating surface at the cartilage-cartilage interface, may be greater than in the intact model. Studies have revealed a strong correlation between the development and initiation of OA over a long period, and contact pressure rises on articular cartilage [95,96].

Our findings of cartilage mechanics while walking and running align with overall trends from earlier computational studies and indirect experimental assessments [97]. The maximum Lagrange strain that we anticipate will occur during the first peak tibiofemoral load during walking (0.22) agrees with the 20% strain measured in the literature [98]. The magnitudes of our anticipated strains also closely matched those in [99], where the authors used a continuum-based finite element model of the knee to apply joint loads estimated from inverse dynamics at four instances of the gait cycle. Our findings concur with earlier simulation studies, suggesting that loads and collagen fiber orientation likely go together. According to these findings, stress increases when collagen fibers are randomly oriented, and superficial cartilage strain decreases along the split line directions parallel to the articular surface during the walking cycle [100,101]. This conclusion is supported by experimental data showing that cartilage's tensile strength is highest when evaluating the split liner pattern perpendicular to the collagen fiber direction [102,103].

However, during the running gait, the highest value for Lagrange strain is generated in the intact model-2 with split-line patterns parallel to the articulating surface, as shown in Figure 8(c), and it indicated the higher risk of OA, as excessive strain contributes to OA [21,28,104]. The maximum fiber stretch is obtained in the deep zone during running gait, whereas a lesser fiber stretch is received in the superficial layer, as illustrated in Figure 5. It may be caused by impact loading in the joint during running; however, the maximum fiber stretch in the superficial zone during walking can be seen in Figure 4. Hence, the fiber stretch values help to predict the gait data [105]. The maximum elastic stresses during walking and running cycle are obtained for models with split-line patterns parallel to the articulating surface for intact models, as shown in Figures 7(b) and 8(b). The study demonstrates that the direction of the cartilage's collagen fibres affects the maximum stress generated and, therefore, is associated with osteoarthritis.

5. Conclusions

The study presents a novel method to control collagen fiber orientation for FRPHE cartilage models for knee joint analysis. This study suggests that during the walking cycle, the maximum contact pressure is observed to be greater in intact models than in OA models; however, during running, the maximum value is more remarkable in OA models than in intact models. Also, the maximum stresses and fluid pressure are obtained for parallel-oriented models than proximal-distal oriented models for both walking and running gait. However, the maximum principal Lagrange strain predicts a similar trend for both intact and OA models throughout the running stance phase; the parallel-oriented models exhibit a higher value than perpendicular and inclined ones. These results will aid researchers in developing improved assistive devices for arthritis patients who engage in subject-specific activities such as walking and running.

Conflicts of Interest

The authors declare that they have no known competing financial interests or personal relationships that could have appeared to influence the work reported in this paper.

Funding

DST-INSPIRE Faculty Award (File No.: DST/INSPIRE/04/2016/000735), Govt. of India

Ethical Approval

Not required

Acknowledgements

The authors gratefully acknowledge the financial support of the DST-INSPIRE Faculty Award, Govt. of India, in executing the computational part of this work.

References

[1] Nuckols RW, Takahashi KZ, Farris DJ, Mizrachi S, Riemer R, Sawicki GS. Mechanics of walking and running up and downhill: A joint-level perspective to guide design of lower-limb exoskeletons. PLoS One 2020;15:1–20. https://doi.org/10.1371/journal.pone.0231996.

[2] Halloran JP, Sibole S, van Donkelaar CC, van Turnhout MC, Oomens CWJ, Weiss JA, et al. Multiscale Mechanics of Articular Cartilage: Potentials and Challenges of Coupling Musculoskeletal, Joint, and Microscale Computational Models. Ann Biomed Eng 2012;40:2456–74. https://doi.org/10.1007/s10439-012-0598-0.

[3] Yao J, Guo N, Xiao Y, Li Z, Li Y, Pu F, et al. Lower limb joint motion and muscle force in treadmill and over-ground exercise. Biomed Eng Online 2019;18:1–12. https://doi.org/10.1186/s12938-019-0708-4.

[4] Thordarson DB. Running biomechanics. Clin Sports Med 1997;16:239–47. https://doi.org/10.1016/S0278-5919(05)70019-3.

[5] Peters AE, Akhtar R, Comerford EJ, Bates KT. Tissue material properties and computational modelling of the human tibiofemoral joint: A critical review. PeerJ 2018;2018:1–48. https://doi.org/10.7717/peerj.4298.

[6] Park S, Krishnan R, Nicoll SB, Ateshian GA. Cartilage interstitial fluid load support in unconfined compression. J Biomech 2003;36:1785–96. https://doi.org/10.1016/S0021-9290(03)00231-8.

[7] Meng Q, An S, Damion RA, Jin Z, Wilcox R, Fisher J, et al. The effect of collagen fibril orientation on the biphasic mechanics of articular cartilage. J Mech Behav Biomed Mater 2017;65:439–53. https://doi.org/10.1016/j.jmbbm.2016.09.001.

[8] Panula HE, Hyttinen MM, Arokoski JPA, Långsjö TK, Pelttari A, Kiviranta I, et al. Articular cartilage superficial zone collagen birefringence reduced and cartilage thickness increased before surface fibrillation in experimental osteoarthritis. Ann Rheum Dis 1998;57:237–45. https://doi.org/10.1136/ard.57.4.237.

[9] Cohen NP, Foster RJ, Mow VC. Composition and dynamics of articular cartilage: Structure, function, and maintaining healthy state. J Orthop Sports Phys Ther 1998;28:203–15. https://doi.org/10.2519/jospt.1998.28.4.203.

[10] Sophia Fox AJ, Bedi A, Rodeo SA. The basic science of articular cartilage: Structure, composition, and function. Sports Health 2009;1:461–8. https://doi.org/10.1177/1941738109350438.
[11] Kazemi M, Li LP, Buschmann MD, Savard P. Partial Meniscectomy Changes Fluid Pressurization in Articular Cartilage in Human Knees. J Biomech Eng 2012;134. https://doi.org/10.1115/1.4005764.
[12] Is O, Guide S, Messier SP, Gutekunst DJ, Davis C, DeVita P, et al. Osteoarthritis as a Chronic Disease. Arthritis Rheum 2005;21:2026–32. https://doi.org/10.1002/art.21139.
[13] Peters AE, Akhtar R, Comerford EJ, Bates KT. The effect of ageing and osteoarthritis on the mechanical properties of cartilage and bone in the human knee joint. Sci Rep 2018;8:1–13. https://doi.org/10.1038/s41598-018-24258-6.
[14] Messier SP. Osteoarthritis of the knee and associated factors of age and obesity: Effects on gait. Med Sci Sports Exerc 1994;26:1446–52. https://doi.org/10.1249/00005768-199412000-00006.
[15] Saxby DJ, Lloyd DG. Osteoarthritis year in review 2016: mechanics. Osteoarthr Cartil 2017;25:190–8. https://doi.org/10.1016/j.joca.2016.09.023.
[16] Klika V, Gaffney EA, Chen YC, Brown CP. An overview of multiphase cartilage mechanical modelling and its role in understanding function and pathology. J Mech Behav Biomed Mater 2016;62:139–57. https://doi.org/10.1016/j.jmbbm.2016.04.032.
[17] Wilson W, Van Donkelaar CC, Van Rietbergen B, Ito K, Huiskes R. Stresses in the local collagen network of articular cartilage: A poroviscoelastic fibril-reinforced finite element study. J Biomech 2004;37:357–66. https://doi.org/10.1016/S0021-9290(03)00267-7.
[18] Korhonen RK, Herzog W. Depth-dependent analysis of the role of collagen fibrils, fixed charges and fluid in the pericellular matrix of articular cartilage on chondrocyte mechanics. J Biomech 2008;41:480–5. https://doi.org/10.1016/j.jbiomech.2007.09.002.
[19] Halonen KS, Mononen ME, Jurvelin JS, Töyräs J, Korhonen RK. Importance of depth-wise distribution of collagen and proteoglycans in articular cartilage-A 3D finite element study of stresses and strains in human knee joint. J Biomech 2013;46:1184–92. https://doi.org/10.1016/j.jbiomech.2012.12.025.
[20] Clark JM. The organisation of collagen fibrils in the superficial zones of articular cartilage. J Anat 1990;171:117–30.
[21] Below S, Arnoczky SP, Dodds J, Kooima C, Walter N. The split-line pattern of the

distal femur: A consideration in the orientation of autologous cartilage grafts. Arthroscopy 2002;18:613–7. https://doi.org/10.1053/jars.2002.29877.
[22] Bursać PM, Obitz TW, Eisenberg SR, Stamenović D. Confined and unconfined stress relaxation of cartilage: appropriateness of a transversely isotropic analysis. J Biomech 1999;32:1125–30. https://doi.org/10.1016/S0021-9290(99)00105-0.
[23] Mononen ME, Mikkola MT, Julkunen P, Ojala R, Nieminen MT, Jurvelin JS, et al. Effect of superficial collagen patterns and fibrillation of femoral articular cartilage on knee joint mechanics-A 3D finite element analysis. J Biomech 2012;45:579–87. https://doi.org/10.1016/j.jbiomech.2011.11.003.
[24] Shirazi R, Shirazi-Adl A, Hurtig M. Role of cartilage collagen fibrils networks in knee joint biomechanics under compression. J Biomech 2008;41:3340–8. https://doi.org/10.1016/j.jbiomech.2008.09.033.
[25] Moger CJ, Arkill KP, Barrett R, Bleuet P, Ellis RE, Green EM, et al. Cartilage collagen matrix reorientation and displacement in response to surface loading. J Biomech Eng 2009;131:1–9. https://doi.org/10.1115/1.3049478.
[26] Sellaro TL, Hildebrand D, Lu Q, Vyavahare N, Scott M, Sacks MS. Effects of collagen fiber orientation on the response of biologically derived soft tissue biomaterials to cyclic loading. J Biomed Mater Res Part A 2007;80A:194–205. https://doi.org/10.1002/jbm.a.30871.
[27] David AC, Carpes FP, Stefanyshyn D. Effects of changing speed on knee and ankle joint load during walking and running. J Sports Sci 2015;33:391–7. https://doi.org/10.1080/02640414.2014.946074.
[28] Halonen KS, Mononen ME, Jurvelin JS, Töyräs J, Kłodowski A, Kulmala JP, et al. Importance of patella, quadriceps forces, and depthwise cartilage structure on knee joint motion and cartilage response during gait. J Biomech Eng 2016;138:1–11. https://doi.org/10.1115/1.4033516.
[29] Mononen ME, Jurvelin JS, Korhonen RK. Implementation of a gait cycle loading into healthy and meniscectomised knee joint models with fibril-reinforced articular cartilage. Comput Methods Biomech Biomed Engin 2015;18:141–52. https://doi.org/10.1080/10255842.2013.783575.
[30] Li J, Hua X, Jones AC, Williams S, Jin Z, Fisher J, et al. The influence of the representation of collagen fibre organisation on the cartilage contact mechanics of the hip joint. J Biomech 2016;49:1679–85. https://doi.org/10.1016/j.jbiomech.2016.03.050.

[31] Pierce DM, Unterberger MJ, Trobin W, Ricken T, Holzapfel GA. A microstructurally based continuum model of cartilage viscoelasticity and permeability incorporating measured statistical fiber orientations. Biomech Model Mechanobiol 2016;15:229–44. https://doi.org/10.1007/s10237-015-0685-x.

[32] Lin J, Shi Y, Men Y, Wang X, Ye J, Zhang C. Mechanical roles in formation of oriented collagen fibers. Tissue Eng - Part B Rev 2020;26:116–28. https://doi.org/10.1089/ten.teb.2019.0243.

[33] Erdemir A. Open Knee: Open Source Modeling and Simulation in Knee Biomechanics. J Knee Surg 2014;29:107–16. https://doi.org/10.1055/s-0035-1564600.

[34] Maas SA, Ellis BJ, Ateshian GA, Weiss JA. FEBio: Finite elements for biomechanics. J Biomech Eng 2012;134. https://doi.org/10.1115/1.4005694.

[35] Yang N, Nayeb-Hashemi H, Canavan PK. The combined effect of frontal plane tibiofemoral knee angle and meniscectomy on the cartilage contact stresses and strains. Ann Biomed Eng 2009;37:2360–72. https://doi.org/10.1007/s10439-009-9781-3.

[36] Venäläinen MS, Mononen ME, Salo J, Räsänen LP, Jurvelin JS, Töyräs J, et al. Quantitative Evaluation of the Mechanical Risks Caused by Focal Cartilage Defects in the Knee. Sci Rep 2016;6:1–12. https://doi.org/10.1038/srep37538.

[37] Morgan EF, Bayraktar HH, Keaveny TM. Trabecular bone modulus-density relationships depend on anatomic site. J Biomech 2003;36:897–904. https://doi.org/10.1016/S0021-9290(03)00071-X.

[38] Donahue TLH, Hull ML, Rashid MM, Jacobs CR. A finite element model of the human knee joint for the study of tibio-femoral contact. J Biomech Eng 2002;124:273–80. https://doi.org/10.1115/1.1470171.

[39] Wong DWC, Chen TLW, Peng Y, Lam WK, Wang Y, Ni M, et al. An instrument for methodological quality assessment of single-subject finite element analysis used in computational orthopaedics. Med Nov Technol Devices 2021;11:100067. https://doi.org/10.1016/j.medntd.2021.100067.

[40] Orozco GA, Tanska P, Mononen ME, Halonen KS, Korhonen RK. The effect of constitutive representations and structural constituents of ligaments on knee joint mechanics. Sci Rep 2018;8:1–15. https://doi.org/10.1038/s41598-018-20739-w.

[41] Chan CW, Rudins A. Foot Biomechanics During Walking and Running. Mayo Clin Proc 1994;69:448–61. https://doi.org/10.1016/S0025-6196(12)61642-5.

[42] Besier TF, Fredericson M, Gold GE, Beaupré GS, Delp SL. Knee muscle forces during walking and running in patellofemoral pain patients and pain-free controls. J Biomech

2009;42:898–905. https://doi.org/10.1016/j.jbiomech.2009.01.032.

[43] Khassetarash A, Vernillo G, Martinez A, Baggaley M, Giandolini M, Horvais N, et al. Biomechanics of graded running: Part II—Joint kinematics and kinetics. Scand J Med Sci Sport 2020;30:1642–54. https://doi.org/10.1111/sms.13735.

[44] Cappellini G, Ivanenko YP, Poppele RE, Lacquaniti F. Motor patterns in human walking and running. J Neurophysiol 2006;95:3426–37. https://doi.org/10.1152/jn.00081.2006.

[45] Li JS, Tsai TY, Felson DT, Li G, Lewis CL. Six degree-of-freedom knee joint kinematics in obese individuals with knee pain during gait. PLoS One 2017;12:1–11. https://doi.org/10.1371/journal.pone.0174663.

[46] David AC, Carpes FP, Stefanyshyn D. Effects of changing speed on knee and ankle joint load during walking and running. J Sports Sci 2015;33:391–7. https://doi.org/10.1080/02640414.2014.946074.

[47] Ko S uk, Stenholm S, Metter EJ, Ferrucci L. Age-associated gait patterns and the role of lower extremity strength – Results from the Baltimore Longitudinal Study of Aging. Arch Gerontol Geriatr 2012;55:474–9. https://doi.org/10.1016/J.ARCHGER.2012.04.004.

[48] Ostrosky KM, VanSwearingen JM, Burdett RG, Gee Z, Eastlack M. A Comparison of Gait Characteristics in Young and Old Subjects. Phys Ther 1994;74:637–44. https://doi.org/10.1093/PTJ/74.7.637.

[49] Ghosh R, Hazra A, Chanda S, Chakraborty D. Computational assessment of growth of connective tissues around textured hip stem subjected to daily activities after THA. Med Biol Eng Comput 2023;61:525–40. https://doi.org/10.1007/s11517-022-02729-3.

[50] Chen Y, Shen Y, Wang K, Qi Y, Niu W, Wang Y. Mechanical analysis of deep tissue injury during sitting in patients with spinal cord injury via parametric finite element model. Biomech Model Mechanobiol 2022;21:1573–84. https://doi.org/10.1007/s10237-022-01607-z.

[51] Schinagl RM, Gurskis D, Chen AC, Sah RL. Depth-dependent confined compression modulus of full-thickness bovine articular cartilage. J Orthop Res 1997;15:499–506. https://doi.org/10.1002/JOR.1100150404.

[52] Todd JN, Maak TG, Ateshian GA, Maas SA, Weiss JA. Hip chondrolabral mechanics during activities of daily living: Role of the labrum and interstitial fluid pressurization. J Biomech 2018;69:113–20. https://doi.org/10.1016/j.jbiomech.2018.01.001.

[53] Reuter T, Hurschler C. Comparison of biphasic material properties of equine articular

cartilage from stress relaxation indentation tests with and without tension-compression nonlinearity. Curr Dir Biomed Eng 2018;4:485–8. https://doi.org/10.1515/cdbme-2018-0116.

[54] Chen X, Zhou Y, Wang L, Santare MH, Wan LQ, Lu XL. Determining Tension–Compression Nonlinear Mechanical Properties of Articular Cartilage from Indentation Testing. Ann Biomed Eng 2016;44:1148–58. https://doi.org/10.1007/s10439-015-1402-8.

[55] Li J. Development and validation of a finite-element musculoskeletal model incorporating a deformable contact model of the hip joint during gait. J Mech Behav Biomed Mater 2021;113:104136. https://doi.org/10.1016/j.jmbbm.2020.104136.

[56] Henak CR, Ateshian GA, Weiss JA. Finite element prediction of transchondral stress and strain in the human hip. J Biomech Eng 2014;136. https://doi.org/10.1115/1.4026101.

[57] Shegaf A, Speirs A. Cartilage Biomechanical Response Differs under Physiological Biaxial Loads and Uniaxial Cyclic Compression. J Biomech Eng 2020;142:1–5. https://doi.org/10.1115/1.4045661.

[58] Tomic A, Grillo A, Federico S. Poroelastic materials reinforced by statistically oriented fibres-numerical implementation and application to articular cartilage. IMA J Appl Math (Institute Math Its Appl 2014;79:1027–59. https://doi.org/10.1093/imamat/hxu039.

[59] Mononen ME, Jurvelin JS, Korhonen RK. Effects of radial tears and partial meniscectomy of lateral meniscus on the knee joint mechanics during the stance phase of the gait cycle - A 3D finite element study. J Orthop Res 2013;31:1208–17. https://doi.org/10.1002/jor.22358.

[60] Li LP, Soulhat J, Buschmann MD, Shirazi-Adl A. Nonlinear analysis of cartilage in unconfined ramp compression using a fibril reinforced poroelastic model. Clin Biomech 1999;14:673–82. https://doi.org/10.1016/S0268-0033(99)00013-3.

[61] Ebrahimi M, Ojanen S, Mohammadi A, Finnilä MA, Joukainen A, Kröger H, et al. Elastic, Viscoelastic and Fibril-Reinforced Poroelastic Material Properties of Healthy and Osteoarthritic Human Tibial Cartilage. Ann Biomed Eng 2019;47:953–66. https://doi.org/10.1007/s10439-019-02213-4.

[62] Holmes MH, Mow VC. The nonlinear characteristics of soft gels and hydrated connective tissues in ultrafiltration. J Biomech 1990;23:1145–56. https://doi.org/10.1016/0021-9290(90)90007-P.

[63] Mononen ME, Julkunen P, Töyräs J, Jurvelin JS, Kiviranta I, Korhonen RK. Alterations in structure and properties of collagen network of osteoarthritic and repaired cartilage modify knee joint stresses. Biomech Model Mechanobiol 2011;10:357–69. https://doi.org/10.1007/s10237-010-0239-1.

[64] Tanska P, Mononen ME, Korhonen RK. A multi-scale finite element model for investigation of chondrocyte mechanics in normal and medial meniscectomy human knee joint during walking. J Biomech 2015;48:1397–406. https://doi.org/10.1016/j.jbiomech.2015.02.043.

[65] Rakhsha M, Smith CR, Recuero AM, Brandon SCE, Vignos MF, Thelen DG, et al. Simulation of surface strain in tibiofemoral cartilage during walking for the prediction of collagen fibre orientation. Comput Methods Biomech Biomed Eng Imaging Vis 2019;7:396–405. https://doi.org/10.1080/21681163.2018.1442751.

[66] Chahine NO, Wang CCB, Hung CT, Ateshian GA. Anisotropic strain-dependent material properties of bovine articular cartilage in the transitional range from tension to compression. J Biomech 2004;37:1251–61. https://doi.org/10.1016/j.jbiomech.2003.12.008.

[67] Huang CY, Stankiewicz A, Ateshian GA, Mow VC. Anisotropy, inhomogeneity, and tension-compression nonlinearity of human glenohumeral cartilage in finite deformation. J Biomech 2005;38:799–809. https://doi.org/10.1016/j.jbiomech.2004.05.006.

[68] Li Q, Han B, Wang C, Tong W, Wei Y, Tseng WJ, et al. Mediation of Cartilage Matrix Degeneration and Fibrillation by Decorin in Post-traumatic Osteoarthritis. Arthritis Rheumatol 2020;72:1266–77. https://doi.org/10.1002/art.41254.

[69] Donahue TLH, Hull ML, Rashid MM, Jacobs CR. A finite element model of the human knee joint for the study of tibio-femoral contact. J Biomech Eng 2002;124:273–80. https://doi.org/10.1115/1.1470171.

[70] Vaziri A, Nayeb-Hashemi H, Singh A, Tafti BA. Influence of meniscectomy and meniscus replacement on the stress distribution in human knee joint. Ann Biomed Eng 2008;36:1335–44. https://doi.org/10.1007/s10439-008-9515-y.

[71] Deneweth JM, Arruda EM, McLean SG. Hyperelastic modeling of location-dependent human distal femoral cartilage mechanics. Int J Non Linear Mech 2015;68:146–56. https://doi.org/10.1016/j.ijnonlinmec.2014.06.013.

[72] Raju V, Koorata PK. Influence of material heterogeneity on the mechanical response of articulated cartilages in a knee joint. Proc Inst Mech Eng Part H J Eng Med

2022;236:1340–8. https://doi.org/10.1177/09544119221116263.

[73] Klets O, Mononen ME, Liukkonen MK, Nevalainen MT, Nieminen MT, Saarakkala S, et al. Estimation of the Effect of Body Weight on the Development of Osteoarthritis Based on Cumulative Stresses in Cartilage: Data from the Osteoarthritis Initiative. Ann Biomed Eng 2018;46:334–44. https://doi.org/10.1007/s10439-017-1974-6.

[74] Bolcos PO, Mononen ME, Mohammadi A, Ebrahimi M, Tanaka MS, Samaan MA, et al. Comparison between kinetic and kinetic-kinematic driven knee joint finite element models. Sci Rep 2018;8:1–11. https://doi.org/10.1038/s41598-018-35628-5.

[75] Wang Y, Fan Y, Zhang M. Comparison of stress on knee cartilage during kneeling and standing using finite element models. Med Eng Phys 2014;36:439–47. https://doi.org/10.1016/j.medengphy.2014.01.004.

[76] Jeffrey JE, Gregory DW, Aspden RM. Matrix Damage and Chondrocyte Viability Following a Single Impact Load on Articular-Cartilage. Arch Biochem Biophys 1995;322:87–96. https://doi.org/10.1006/ABBI.1995.1439.

[77] Wilson W, van Burken C, van Donkelaar CC, Buma P, van Rietbergen B, Huiskes R. Causes of mechanically induced collagen damage in articular cartilage. J Orthop Res 2006;24:220–8. https://doi.org/10.1002/JOR.20027.

[78] Shirazi R, Shirazi-Adl A. Computational biomechanics of articular cartilage of human knee joint: Effect of osteochondral defects. J Biomech 2009;42:2458–65. https://doi.org/10.1016/j.jbiomech.2009.07.022.

[79] Haris A, Beng Chye Tan V. Stress response envelopes of intact tibiofemoral joint and knee osteoarthritis. Proc Inst Mech Eng Part H J Eng Med 2020;234:1151–61. https://doi.org/10.1177/0954411920944078.

[80] Raju V, Koorata PK, Kamat Y. Case study for contact pressure improvisation with graded implant material in articular cartilages of knee joint. J Mech Sci Technol 2021;35:1049–54. https://doi.org/10.1007/s12206-021-0218-8.

[81] Thambyah A, Goh JCH, Das De S. Contact stresses in the knee joint in deep flexion. Med Eng Phys 2005;27:329–35. https://doi.org/10.1016/j.medengphy.2004.09.002.

[82] Halonen KS, Mononen ME, Jurvelin JS, Töyräs J, Salo J, Korhonen RK. Deformation of articular cartilage during static loading of a knee joint - Experimental and finite element analysis. J Biomech 2014;47:2467–74. https://doi.org/10.1016/j.jbiomech.2014.04.013.

[83] Sylvia MK, Czapla NA, Lerner ZF, Tuttle DJ, Otto J, Hazelwood SJ, et al. Development of a Human Knee Joint Finite Element Model To Investigate Cartilage

Stress During Walking in Obese and Normal Weight Adults 2015:1–2.

[84] Esrafilian A, Stenroth L, Mononen ME, Tanska P, Van Rossom S, Lloyd DG, et al. 12 Degrees of Freedom Muscle Force Driven Fibril-Reinforced Poroviscoelastic Finite Element Model of the Knee Joint. IEEE Trans Neural Syst Rehabil Eng 2021;29:123–33. https://doi.org/10.1109/TNSRE.2020.3037411.

[85] Esrafilian A, Stenroth L, Mononen ME, Tanska P, Avela J, Korhonen RK. EMG-Assisted Muscle Force Driven Finite Element Model of the Knee Joint with Fibril-Reinforced Poroelastic Cartilages and Menisci. Sci Rep 2020;10:1–16. https://doi.org/10.1038/s41598-020-59602-2.

[86] Erbulut DU, Sadeqi S, Summers R, Goel VK. Tibiofemoral Cartilage Contact Pressures in Athletes During Landing: A Dynamic Finite Element Study. J Biomech Eng 2021;143. https://doi.org/10.1115/1.4051231.

[87] El-Rich M. Orthopedic biomechanics: stress analysis. Hum Orthop Biomech Fundam Devices Appl 2022:25–37. https://doi.org/10.1016/B978-0-12-824481-4.00008-1.

[88] Hyodo K, Kanamori A, Kadone H, Takahashi T, Kajiwara M, Yamazaki M. Gait Analysis Comparing Kinematic, Kinetic, and Muscle Activation Data of Modern and Conventional Total Knee Arthroplasty. Arthroplast Today 2020;6:338–42. https://doi.org/10.1016/j.artd.2020.03.011.

[89] Roberts M, Mongeon D, Prince F. Biomechanical parameters for gait analysis: a systematic review of healthy human gait. Phys Ther Rehabil 2017;4:6. https://doi.org/10.7243/2055-2386-4-6.

[90] Hall M, Stevermer CA, Gillette JC. Gait analysis post anterior cruciate ligament reconstruction: Knee osteoarthritis perspective. Gait Posture 2012;36:56–60. https://doi.org/10.1016/j.gaitpost.2012.01.003.

[91] Abid M, Mezghani N, Mitiche A. Knee joint biomechanical gait data classification for knee pathology assessment: A literature review. Appl Bionics Biomech 2019;2019. https://doi.org/10.1155/2019/7472039.

[92] Schliemann B, Glasbrenner J, Rosenbaum D, Lammers K, Herbort M, Domnick C, et al. Changes in gait pattern and early functional results after ACL repair are comparable to those of ACL reconstruction. Knee Surgery, Sport Traumatol Arthrosc 2018;26:374–80. https://doi.org/10.1007/s00167-017-4618-3.

[93] Adouni M, Shirazi-Adl A, Shirazi R. Computational biodynamics of human knee joint in gait: From muscle forces to cartilage stresses. J Biomech 2012;45:2149–56. https://doi.org/10.1016/j.jbiomech.2012.05.040.

[94] Bennett HJ, Valenzuela KA, Lynn SK, Weinhandl JT. Foot Rotation Gait Modifications Affect Hip and Ankle, but Not Knee, Stance Phase Joint Reaction Forces during Running. J Biomech Eng 2021;143. https://doi.org/10.1115/1.4047994.

[95] Maxian T a, Brown TD, Weinstein SL. Chronic stress tolerance levels for human articular cartilage: Two nonuniform contact models applied to long-term follow-up of CDH. J Biomech 1995;28:159–66. https://doi.org/10.1016/0021-9290(94)00054-8.

[96] Hadley NA, Brown TD, Weinstein SL. The effects of contact pressure elevations and aseptic necrosis on the long-term outcome of congenital hip dislocation. J Orthop Res 1990;8:504–13. https://doi.org/10.1002/jor.1100080406.

[97] Lad NK, Liu B, Ganapathy PK, Utturkar GM, Sutter EG, Moorman CT, et al. Effect of normal gait on in vivo tibiofemoral cartilage strains. J Biomech 2016;49:2870–6. https://doi.org/10.1016/J.JBIOMECH.2016.06.025.

[98] Liu F, Kozanek M, Hosseini A, Van de Velde SK, Gill TJ, Rubash HE, et al. In vivo tibiofemoral cartilage deformation during the stance phase of gait. J Biomech 2010;43:658–65. https://doi.org/10.1016/J.JBIOMECH.2009.10.028.

[99] Shim VB, Besier TF, Lloyd DG, Mithraratne K, Fernandez JF. The influence and biomechanical role of cartilage split line pattern on tibiofemoral cartilage stress distribution during the stance phase of gait. Biomech Model Mechanobiol 2016;15:195–204. https://doi.org/10.1007/s10237-015-0668-y.

[100] Shim VB, Besier TF, Lloyd DG, Mithraratne K, Fernandez JF. The influence and biomechanical role of cartilage split line pattern on tibiofemoral cartilage stress distribution during the stance phase of gait. Biomech Model Mechanobiol 2016;15:195–204. https://doi.org/10.1007/s10237-015-0668-y.

[101] Mononen ME, Mikkola MT, Julkunen P, Ojala R, Nieminen MT, Jurvelin JS, et al. Effect of superficial collagen patterns and fibrillation of femoral articular cartilage on knee joint mechanics—A 3D finite element analysis. J Biomech 2012;45:579–87. https://doi.org/10.1016/J.JBIOMECH.2011.11.003.

[102] Kempson GE, Muir H, Pollard C, Tuke M. The tensile properties of the cartilage of human femoral condyles related to the content of collagen and glycosaminoglycans. Biochim Biophys Acta - Gen Subj 1973;297:456–72. https://doi.org/10.1016/0304-4165(73)90093-7.

[103] Sasazaki Y, Shore R, Seedhom BB. Deformation and failure of cartilage in the tensile mode. J Anat 2006;208:681–94. https://doi.org/10.1111/J.1469-7580.2006.00569.X.

[104] Kazemi M, Dabiri Y, Li LP. Recent advances in computational mechanics of the

human knee joint. Comput Math Methods Med 2013;2013. https://doi.org/10.1155/2013/718423.

[105] Dhaher YY, Kwon TH, Barry M. The effect of connective tissue material uncertainties on knee joint mechanics under isolated loading conditions. J Biomech 2010;43:3118–25. https://doi.org/10.1016/j.jbiomech.2010.08.005.